PHYSICAL REVIEW B **81**, 041309(R) (2010)

Direct mapping of the spin-filtered surface bands of a three-dimensional quantum spin Hall insulator

Akinori Nishide,[1] Alexey A. Taskin,[2] Yasuo Takeichi,[1] Taichi Okuda,[1] Akito Kakizaki,[1] Toru Hirahara,[3] Kan Nakatsuji,[1] Fumio Komori,[1] Yoichi Ando,[2,*] and Iwao Matsuda[1,†]

[1]*Institute for Solid State Physics, The University of Tokyo, Kashiwa, Chiba 277-8581, Japan*

[2]*Institute of Scientific and Industrial Research, Osaka University, Ibaraki, Osaka 567-0047, Japan*

[3]*Department of Physics, School of Science, The University of Tokyo, Bunkyo-ku, Tokyo 113-0033, Japan*

(Received 11 February 2009; revised manuscript received 6 October 2009; published 26 January 2010)

Spin-polarized band structure of the three-dimensional quantum spin Hall insulator $Bi_{1-x}Sb_x$ (x=0.12–0.13) was fully elucidated by spin-polarized angle-resolved photoemission spectroscopy using a high-yield spin polarimeter equipped with a high-resolution electron spectrometer. Between the two time-reversal-invariant points, $\bar{\Gamma}$ and $\bar{M}$, of the (111) surface Brillouin zone, a spin-up band (Σ_1' band) was found to cross the Fermi energy only once, providing unambiguous evidence for the strong topological insulator phase. The observed spin-polarized band dispersions determine the "mirror chirality" to be −1, which agrees with the theoretical prediction based on first-principles calculations.

DOI: 10.1103/PhysRevB.81.041309 PACS number(s): 73.20.−r, 72.25.Dc, 73.43.Fj, 79.60.−i

The spin Hall effect, which makes it possible to produce spin currents without magnet, has recently attracted a lot of attention for its potential impact on future spintronics.[1,2] The spin Hall effect has also stimulated physicists not only to understand the intriguing phenomena, but also to extend the theoretical frameworks to the "quantum spin Hall" (QSH) effect,[3–6] which is realized in a topologically nontrivial electronic state, as in the case of the quantum Hall effect. The theories of QSH effect have been constructed for two and three dimensions, and experimentalists have already attempted to obtain evidence for those topologically nontrivial states of matter. The QSH phase in two dimensions is gapped in the bulk but is gapless for edge modes. Unlike the spin itself, the spin current is time-reversal invariant. Hence, these modes carry spin currents without breaking time-reversal symmetry. Furthermore, the edge modes are robust against disorder or modest changes in boundary conditions, such as surface roughness or nonmagnetic impurities. The Z_2 topological number ν, which represents the number of Kramers pairs in the edge states, characterizes this topological protection[7,8] in two dimensions and distinguishes the topological insulator (ν=1) from an ordinary insulator (ν=0). This two-dimensional (2D) QSH phase has been theoretically proposed to be realized in bismuth bilayers[5] and in CdTe/HgTe/CdTe quantum wells.[9] In the latter case, the edge states were indeed observed in recent transport experiments.[10]

In three dimensions, there are four Z_2 invariants ($\nu_0;\nu_1\nu_2\nu_3$), representing time-reversal-invariant band structures.[7,8] When ν_0=1, the system is a three-dimensional (3D) strong topological insulator, where the "edge states" (i.e., 2D surface states) form a Kramers pair of opposite spin currents flowing on a surface (Fig. 1) and are robust against disorder.[11–13] The spin lies within the surface plane and is perpendicular to the momentum (wave number) of the electron. The existence of such spin-current pairs is in sharp contrast to the trivial insulator where ($\nu_0;\nu_1\nu_2\nu_3$)=(0;000). Recently, the semiconductor alloy $Bi_{1-x}Sb_x$ ($x\sim0.1$) was predicted[12] to be a strong topological insulator, and subsequently a spin-integrated photoemission study has mapped the (111) surface states of this system at x=0.10 to find a trace of the predicted topological band structure.[14] However, since the surface states of topological insulators are expected to be spin polarized (SP), the spin characters of all the edge states in the surface Brillouin zone would need to be clarified for a complete proof of the 3D QSH phase. On the theoretical front, predictions for the surface states of $Bi_{1-x}Sb_x$ based on a tight-binding model and first-principles calculations differ in a fundamental way, giving different mirror chirality η (Ref. 15); since the existing data for the surface state of $Bi_{1-x}Sb_x$ (Ref. 14) fail to elucidate η, its experimental determination is strongly called for. Therefore, it is important to conduct direct measurements of spin-polarized surface-state bands on the $Bi_{1-x}Sb_x$ crystals by spin- and angle-resolved photoemission spectroscopy (SARPES). In the present work, we took advantage of our spin-polarized photoemission spec-

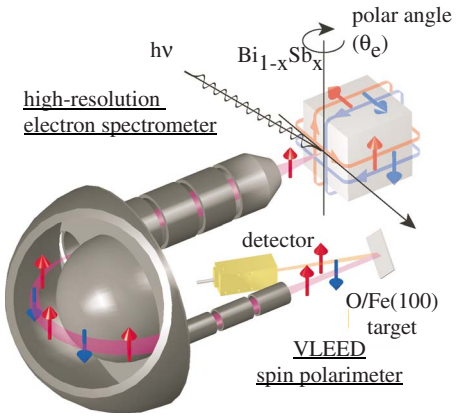

FIG. 1. (Color online) Schematic drawing of the high-resolution SARPES measurements. SP electrons are depicted as up (red) and down (blue) arrows. Spin currents are also depicted for the edge states in the 3D quantum spin Hall phase, from which the SP photoelectrons are emitted into a high-resolution electron spectrometer and the high-yield VLEED spin polarimeter.

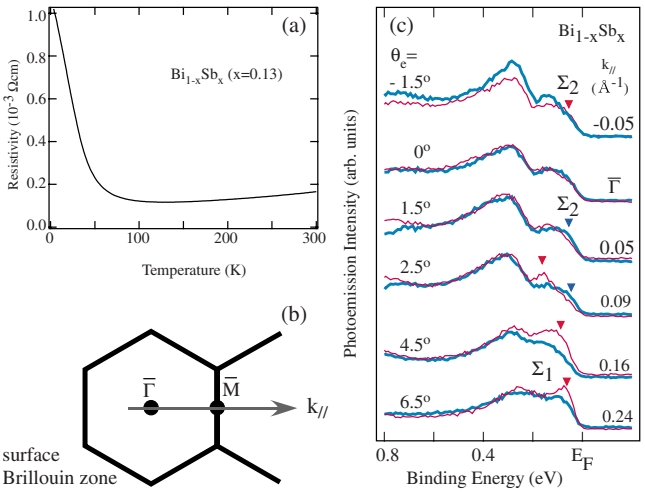

FIG. 2. (Color online) (a) Temperature dependence of the resistivity of the present $Bi_{1-x}Sb_x$ (x=0.13) sample. (b) The (111) surface Brillouin zone of $Bi_{1-x}Sb_x$ with high symmetry points and the direction of the wave number $k_{\|}$, which indicates the angle-scanning direction in the present photoemission experiment. (c) SARPES spectra, $I_{\uparrow}$ (thin line, colored in red) and $I_{\downarrow}$ (thick line, colored in blue), of a $Bi_{1-x}Sb_x$ (x=0.12) crystal at various emission angles θ_e and corresponding $k_{\|}$ values. Peak positions of the surface states, Σ_1 and Σ_2, are indicated by triangles.

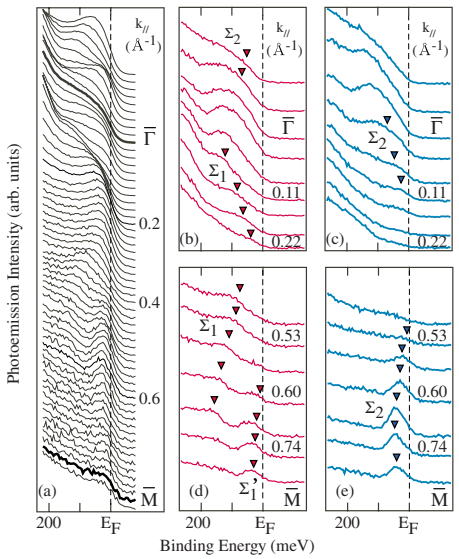

FIG. 3. (Color online) (a) A sequence of spin-integrated ARPES spectra of Bi_xSb_{1-x} (x=0.13) along the $\bar{\Gamma}$-$\bar{M}$ line. [(b) and (c)] SARPES spectra of (b) $I_{\uparrow}$ (thin line, colored in red) and (c) $I_{\downarrow}$ (thick line, colored in blue) for Bi_xSb_{1-x} (x=0.12) near $\bar{\Gamma}$. [(d) and (e)] SARPES spectra of (d) $I_{\uparrow}$ and (e) $I_{\downarrow}$ near $\bar{M}$. Peak positions of the surface state, Σ_1, Σ_2, and Σ_1', are indicated by triangles.

trometer with a high spin-polarimetry efficiency and a high energy resolution,[16] and we determined all the spin-polarized bands of $Bi_{1-x}Sb_x$ (x=0.12–0.13). Our results provide direct evidence for the QSH phase in the 3D topological insulator and clarifies the mirror chirality η, settling the essential topological structure of the surface states of this material.

$Bi_{1-x}Sb_x$ (x=0.12–0.13) crystals were grown from a stoichiometric mixture of 99.9999% purity Bi and Sb elements by a zone melting method. As shown in Fig. 2(a), the resistivity of the present $Bi_{1-x}Sb_x$ (x=0.13) crystals below 100 K increased monotonically with decreasing temperature. This temperature dependence of the electrical resistivity signifies the presence of a bulk gap or a bulk-insulating nature of the sample crystals, being consistent with the published data in the literature for similar x values.[14] The crystals were cleaved along the (111) plane at 123 K below 3×10^{-8} Pa. The SARPES was performed at BL-19A (KEK-PF, Japan) with a high-resolution hemispherical analyzer (SPECS Phoibos-150) equipped with a homemade high-yield spin-polarimeter using spin-dependent very-low-energy electron diffraction (VLEED).[16]

The measurement setup is schematically drawn in Fig. 1. SARPES spectra were recorded with energy and angle resolutions of 50 meV and ±1°, respectively. In the VLEED detector, the spin polarization P is acquired from the intensities of the reflected electrons interacted with the majority-spin (minority-spin) states of the Fe(001)$p(1\times1)$-O target, I_{maj} (I_{min}), by $P=(1/S_{eff})[(I_{maj}-I_{min})/(I_{maj}+I_{min})]$. Here, $S_{eff}=0.32\pm0.04$ is the effective Sherman function, which was determined by preceding measurement of the polarization of secondary electrons from Fe(001). The use of the ferromagnetic Fe crystal surface covered with oxide atomic layer enables stable spin detections with high yields. From I_{maj} and I_{min}, the spin-up and -down spectra are obtained by $I_{\uparrow,\downarrow}=(I_{maj}+I_{min})(1\pm P)/2$. For comparison, spin-integrated ARPES spectra were measured with a hemispherical analyzer (VG Scienta SES-100) at energy and angle resolutions of 30 meV and ±0.2°. All the ARPES spectra were taken at 120–140 K with a He $I\alpha$ source along the $\bar{\Gamma}$-$\bar{M}$ line in the (111) surface Brillouin zone shown in Fig. 2(b). Figure 2(c) shows typical SARPES spectra of $Bi_{1-x}Sb_x$ (x=0.12) at various wave numbers $k_{\|}$, converted from the emission angle θ_e, where spin-dependent spectral features can be distinctively seen in the $I_{\uparrow}$ (thin red line) and $I_{\downarrow}$ (thick blue line) plots. Photoemission peaks assigned to the surface states are located at binding energies E_B of less than 0.2 eV and are indicated by triangles. Labeling of the surface states in Fig. 2(c) was adopted from Ref. 15.

Figure 3(a) shows the spin-integrated ARPES spectra near E_F along the $\bar{\Gamma}$-$\bar{M}$ line. Dispersions of the surface-state bands are clearly resolved as in the previous report.[14] Figures 3(b)–3(e) present the SARPES spectra of $I_{\uparrow}$ [Figs. 3(b) and 3(d)] and $I_{\downarrow}$ [Figs. 3(c) and 3(e)] for each band near the $\bar{\Gamma}$ and $\bar{M}$ points. In Figs. 3(b)–3(e), peak positions of the surface state, Σ_1, Σ_2, and Σ_1', are indicated by triangles. The spectral features near the $\bar{\Gamma}$ point are mainly assigned to the insulating bulk band. The bulk bands were distinguished from the surface bands by their incident-photon-energy dependence, as was done in Ref. 14. Note that the bulk band structure of $Bi_{1-x}Sb_x$ is already well understood, as summarized in Ref. 17, and it changes only gradually upon Sb doping, which is consistent with our observation. The Σ_2 band, dispersing from the $\bar{\Gamma}$ point, crosses E_F at around $k_{\|}=0.1$ Å^{-1}, indicating a metallic nature. The photoemission intensity of the Σ_2 band is observed with positive wave num-

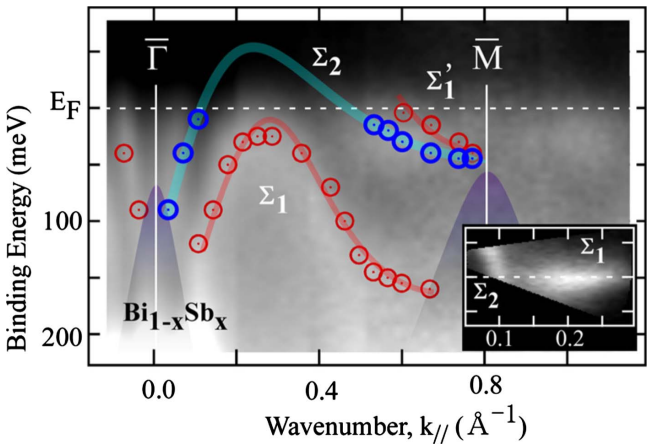

FIG. 4. (Color online) Spin-polarized band dispersions of the surface states of $Bi_{1-x}Sb_x$ (x=0.12–0.13). The spin-resolved data are plotted with open circles and overlaid on a spin-integrated grayscale diagram. Spin-up (spin-down) bands plotted with thin red (thick blue) circles and their dispersion curves are schematically traced by thin (thick) lines. The bulk band projection, tentatively estimated from the ARPES data, is shown as the shaded purple area. The inset shows two-dimensional wave-number-resolved photoemission intensity map at the Fermi level of $Bi_{1-x}Sb_x$ (x=0.13). The dashed line is along the $\bar{\Gamma}$-$\bar{M}$ axis.

bers in the $I_\downarrow$ spectra in Fig. 3(c) and, therefore, Σ_2 has the spin-down polarization. On the other hand, the Σ_1 band, which shows up in the $I_\uparrow$ spectra [Fig. 3(b)] and thus has the spin-up polarization, approaches E_F from $\bar{\Gamma}$ and it disperses back as $k_\parallel$ increases toward $\bar{M}$ as found in Fig. 3(a). In the $I_\downarrow$ data in Fig. 3(e), a band appears at E_F around 0.5 Å^{-1} and it disperses slightly to higher E_B. Since this band has the spin-down polarization, it is likely assigned to Σ_2. Near the $\bar{M}$ point, the Σ_1' band crosses E_F in the $I_\uparrow$ spectra in Fig. 3(d). These two metallic bands with opposite spin polarizations, Σ_2 of down spin and Σ_1' of up spin, converge at the $\bar{M}$ point.

Figure 4 shows a dispersion plot of the spin-polarized surface-state bands obtained from the SARPES spectra in Figs. 3(b)–3(e). For comparison, the data are displayed on a grayscale band diagram constructed from the spin-integrated ARPES spectra shown in Fig. 3(a). While the band structure is essentially similar to the one reported previously,[14] it is now found to be basically composed of three surface-state bands, Σ_1, Σ_2, and Σ_1'. The Σ_2 band, creating an electron pocket at the $\bar{\Gamma}$ point with the Fermi wave number k_F of 0.1 Å^{-1}, has asymmetric spin polarization with respect to $\bar{\Gamma}$. The Σ_1 band disperses toward E_F and returns to higher E_B without showing clear E_F crossing, which has been also confirmed by a photoemission Fermi-surface mapping of the relevant part of the Brillouin zone, as shown in the inset to Fig. 4. The intensity at the Fermi level, corresponding to the Σ_1 band, was a tail of the spectral-weight peaks, as shown in Fig. 3(a). Namely, the top of the Σ_1 band is found to indeed lie below E_F; this is slightly different from the previous result,[14] in which the Σ_1 band obviously crossed E_F and formed a small hole pocket. The slight shift of the E_F position is likely due to the difference in the Sb concentration (x=0.10 in Ref. 14, while x=0.12–0.13 in the present work), which could lead to a chemical-potential shift. The Σ_2 band appears again at E_F near the midpoint of the $\bar{\Gamma}$-$\bar{M}$ line and forms an electron pocket around $\bar{M}$. The dispersion of the Σ_1' band is very close to that of the Σ_2 band and the two bands are hardly distinguishable in the spin-integrated spectra, as shown in the grayscale diagram in Fig. 4. However, these two bands have opposite spin polarizations and, therefore, their dispersion can be unambiguously resolved in the spin-revolved spectra and plotted as the two spin-polarized bands in Fig. 4. While the previous photoemission work[14] reported a degeneracy of the Σ_2 and Σ_1' bands at E_F, they actually intersect with E_F at different wave numbers, $k_F \sim 0.5$ Å^{-1} for Σ_2 and $k_F \sim 0.6$ Å^{-1} for Σ_1' (Fig. 4). The Σ_1' band also creates an electron pocket around $\bar{M}$ and it converges with Σ_2 at $\bar{M}$, which is natural because these two bands have opposite spin polarities and the spin polarization P must disappear at the time-reversal-invariant point $\bar{M}$. Those spin properties demonstrated in Fig. 4 are typical for a compound with a large spin-orbit coupling, whose surface states are generally spin split due to the loss of space inversion symmetry (Rashba effect). The Kramers theorem dictates that the spin-split states become degenerate at the symmetry points, $\bar{\Gamma}$ and $\bar{M}$, and the spin structure naturally becomes antisymmetric with respect to these points.

Based on the Z_2 topology, structures of bulk insulators are classified into trivial and nontrivial cases by examining the parity of the valence bands. Furthermore, it has been shown that counting the number of surface-band crossings at E_F gives a convenient way to distinguish the two: odd and even numbers of surface-band crossings correspond to the nontrivial and trivial cases, respectively. The clear spin-polarized band structure shown in Fig. 4 signifies three E_F crossings (odd number of times) for the spin-split surface states. Consequently, one can unambiguously conclude that $Bi_{1-x}Sb_x$ (x=0.12–0.13) is a topological insulator belonging to a nontrivial class, as predicted theoretically.[12] It should be noted that the previous spin-integrated experiment[14] reached the same conclusion, although the number of the E_F crossings was different. The present study not only disentangled the complicated band structure suggested in Ref. 14, but also unambiguously elucidated which of the many bands represents the topologically nontrivial nature; in the present case, it is the Σ_1' band that makes $Bi_{1-x}Sb_x$ a strong topological insulator.

Now let us discuss the implications of the present results. Two theoretical approaches[18,19] have been employed for calculating the surface-band structure of $Bi_{1-x}Sb_x$. One was based on first-principles calculations, but was restricted to a slab or a thin-film geometry, so that the result left some ambiguity regarding the size effect.[19] The other was a tight-binding model for a semi-infinite system, but the results strongly depended on the phenomenological band parameters.[18] These two approaches were both applied to the Bi(111) surface and yielded incompatible surface spin band structures.[15,20] A recent SARPES experiment on pure Bi confirmed the spin-polarized surface-band dispersions predicted by the first-principles calculations,[21] which suggested that

the former approach is likely to be appropriate for pure Bi, but the situation has not been clear for $Bi_{1-x}Sb_x$ in the QSH phase. Recently, partly to address this issue, two new topological invariants, mirror Chern number and mirror chirality, have been introduced,[15] which is analogous to the spin Chern number defined in the 2D QSH state in graphene.[7,8] The main distinction in the band structures predicted by the two approaches is the presence of a crossing point (Dirac point) of the spin-split surface bands, Σ_1 and Σ_2, that are filled at the two symmetry points, $\bar{\Gamma}$ and $\bar{M}$.[15] The mirror chirality η, which is derived from the mirror Chern number, is +1 for the crossing case (tight-binding model) and −1 for the noncrossing case (first-principles calculations).[15] As is clear in Fig. 4, the Σ_1 and Σ_2 bands do not cross each other, which leads to the conclusion that $\eta=-1$ and the first-principles approach is likely to be appropriate. Intriguingly, this implies that the g factor is negative in the 3D QSH phase of $Bi_{1-x}Sb_x$, which has also been indirectly inferred for pure Bi (Ref. 15) from the SARPES data.[21] It is useful to note that the spin-resolved surface-band structure elucidated here is consistent with a theoretical approach[20] which considers the hybridization between the topological surface state and other trivial surface states. Finally, we note that after the initial submission of this Rapid Communication, a related paper was published.[22] The experiment reported in Ref. 22 determined the spin polarizations only for the Σ_1 and Σ_2 bands around the $\bar{\Gamma}$ point, and it failed to address the crucial Σ_1' band. Nevertheless, what is reported in Ref. 22 is consistent with our complete picture.

In conclusion, our high-resolution SARPES study elucidated the spin-polarized surface-band structures of $Bi_{1-x}Sb_x$ ($x=0.12-0.13$), giving unambiguous evidence that this system is a 3D strong topological insulator. Furthermore, we were able to determine the mirror chirality of this system to be −1, which excludes the existence of a Dirac point in the middle of the $\bar{\Gamma}$-$\bar{M}$ line. The measured surface states are the edge states of the 3D quantum spin Hall phase, providing robust spin-current pairs at the surface. The SARPES measurement with an energy resolution below 50 meV is one of the critical techniques for complementing the topological band theory for spins and spin currents.

Shuichi Murakami is gratefully acknowledged for valuable comments and discussions. This work was partly supported by JSPS (KAKENHI Grants No. 18360018, No. 19340078, No. 13674002, and No. 2003004) and by AFOSR (Grant No. AOARD-08-4099).

*y_ando@sanken.osaka-u.ac.jp
†imatsuda@issp.u-tokyo.ac.jp

[1] S. Murakami, N. Nagaosa, and S.-C. Zhang, Science **301**, 1348 (2003).
[2] J. Sinova, D. Culcer, Q. Niu, N. A. Sinitsyn, T. Jungwirth, and A. H. MacDonald, Phys. Rev. Lett. **92**, 126603 (2004).
[3] B. A. Bernevig and S.-C. Zhang, Phys. Rev. Lett. **96**, 106802 (2006).
[4] D. N. Sheng, Z. Y. Weng, L. Sheng, and F. D. M. Haldane, Phys. Rev. Lett. **97**, 036808 (2006).
[5] S. Murakami, Phys. Rev. Lett. **97**, 236805 (2006).
[6] S. Murakami and S. I. Kuga, Phys. Rev. B **78**, 165313 (2008).
[7] C. L. Kane and E. J. Mele, Phys. Rev. Lett. **95**, 146802 (2005).
[8] C. L. Kane and E. J. Mele, Phys. Rev. Lett. **95**, 226801 (2005).
[9] B. A. Bernevig, T. L. Hughes, and S.-C. Zhang, Science **314**, 1757 (2006).
[10] M. Konig *et al.*, Science **318**, 766 (2007).
[11] S. Murakami, New J. Phys. **9**, 356 (2007).
[12] L. Fu and C. L. Kane, Phys. Rev. B **76**, 045302 (2007).
[13] L. Fu, C. L. Kane, and E. J. Mele, Phys. Rev. Lett. **98**, 106803 (2007).
[14] D. Hsieh *et al.*, Nature (London) **452**, 970 (2008).
[15] J. C. Y. Teo, L. Fu, and C. L. Kane, Phys. Rev. B **78**, 045426 (2008).
[16] T. Okuda *et al.*, Rev. Sci. Instrum. **79**, 123117 (2008).
[17] B. Lenoir *et al.*, J. Phys. Chem. Solids **57**, 89 (1996).
[18] Y. Liu and R. E. Allen, Phys. Rev. B **52**, 1566 (1995).
[19] S. Golin, Phys. Rev. **166**, 643 (1968).
[20] H.-J. Zhang, C. X. Liu, X. L. Qi, X. Y. Deng, X. Dai, S. C. Zhang, and Z. Fang, Phys. Rev. B **80**, 085307 (2009).
[21] T. Hirahara *et al.*, New J. Phys. **10**, 083038 (2008).
[22] D. Hsieh *et al.*, Science **323**, 919 (2009).